Differential Power Based Selective Phase Tripping for Fault-resilient Microgrid

Bhatraj Anudeep and Paresh Kumar Nayak

Abstract—Modern fault-resilient microgrids (MGs) require the operation of healthy phases during unbalanced short-circuits to improve the system reliability. This study proposes a differential power based selective phase tripping scheme for MGs consisting of synchronous and inverter-interfaced distributed generators (DGs). First, the differential power is computed using the line-end superimposed voltage and current signals. Subsequently, to make the scheme threshold-free, a power coefficient index is derived and used for identifying faulted phases in an MG. The protection scheme is tested on a standard MG operating in either grid-connected or islanding mode, which is simulated using PSCAD/EMTDC. The efficacy of the scheme is also assessed on the OPAL-RT manufactured real-time digital simulation (RTDS) platform. Further, the performance of the proposed protection scheme is compared with a few existing methods. The results show that the selective tripping of faulted phases in MGs can be achieved quickly and securely using the proposed scheme.

Index Terms—Distributed generator, differential power, fault detection, microgrid protection, selective phase tripping.

I. INTRODUCTION

THE generation of electric power in low- and medium-voltage distribution systems using wind and photovoltaic distributed generators (PVDGs) continues to increase progressively worldwide [1], [2]. However, owing to the intermittent nature of these distributed generators (DGs), it is difficult to manage their direct connection into the distribution network, especially when the penetration level of DGs is high. Microgrids (MGs), which are low-voltage grids, have gained popularity for integrating DGs into distribution systems. The MGs have the flexibility of operating in either grid-connected or islanding mode. The advantages of MGs over traditional distribution networks include the uninterrupted power supply to consumers, as well as improved reliability and power quality [3]. However, the operation modes of MGs consisting of inverter-interfaced DGs not only alter the fault current level but also change the unidirectional power flow of the traditional radial distribution systems into bidirectional power flow [4], [5]. Consequently, it is difficult to de-

tect and isolate faults correctly in MGs using traditional overcurrent relay based protection approaches for radial distribution networks [6].

To overcome the limitations of traditional overcurrent relays, several advanced relaying schemes based on adaptive principles [7] - [9] and communication-assisted techniques [10], [11] have been proposed for the fast and reliable detection and isolation of faults in MGs. However, these protection schemes are not suitable for the selective phase tripping of unbalanced short-circuits in MGs. In modern fault-resilient MGs, selective phase tripping is essential for unbalanced short-circuits to enhance the system reliability [12] - [15]. Selective phase tripping requires the correct identification of the fault type and phase [16].

In recent years, efforts have been devoted to the fast and correct identification of fault type or phase in modern fault-resilient MGs through single- and double-pole trippings. In [17], the cross-alienation coefficients, based on the faulted phase identification (FPI) algorithm, are proposed for MGs using the line-end synchronized current signals. In [18], a complete protection solution is proposed for low-voltage alternating current (AC) MGs using the spectral energy of the differential current component derived through the sparse Fourier kernel fast time-frequency transform. In [19], a communication-assisted relay algorithm is proposed to detect and classify faults in isolated MGs consisting of inverter-based DGs. In this scheme, the fault classification is performed based on multiple features calculated from the line-end current waveforms through the random forest algorithm.

The differential energy derived from the line-end current signals through the S-transform is used in [20] to detect and isolate fault phases in MGs. A fault-resistance method based on the active power of zero- or d-frame component consumed by fault resistance is proposed in [21] to protect AC MGs. Another FPI algorithm is proposed in [22] for MGs using the line-end current signals processed through the S-transform and artificial neural network (ANN). A decision tree (DT)-based differential protection scheme in [23] and a combined wavelet transform (WT) and DT-based relay algorithm in [24] are proposed for MGs. Another relay algorithm is proposed in [25] to detect and classify faults in MGs based on the features derived from the relay-end current signals through wavelet singular entropy and fuzzy logic. The fault detection and classification in MGs is performed based on the differential features derived from the line-end current signals through the Hilbert-Huang transform and machine learning technique [26]. In [27], a communication-assisted microprocessor-based relaying scheme with single-phase trip-

ping capability is proposed for MGs using line-end synchronized voltage and current signals.

The aforementioned studies have reported various methods to detect and isolate faulted phases in MGs. However, in most cases, their efficacies have not been tested in grid-connected and islanding operation modes, critical fault cases (high-resistance faults and high-impedance faults (HIFs) with low-arcing currents), and non-fault switching transients (large load switching, capacitor switching, DG outage, line outage, etc.). In addition, the feasibility of the practical implementation of the most available protection schemes have not been evaluated through a real-time digital platform. Further, retraining is necessary for training-based protection schemes such as ANN and DT to cope with significant changes in system configurations, which frequently occur in MGs. Considering the above deficiencies, a fast and secure differential power based selective phase tripping scheme is proposed in this study to improve the system reliability of modern MGs.

The main contributions of this study for the effective detection and isolation of fault phases in MGs can be summarized as follows.

1) This study introduces a differential power based fault detection scheme for MGs using the measured three-phase voltage and current signals at the relay location.

2) A threshold-free power coefficient index derived from the line-end differential power is introduced to identify the fault phase in MGs.

3) The performance of the proposed protection scheme is evaluated in numerous fault and non-fault cases generated in a standard test MG system using the PSCAD/EMTDC software.

4) Based on the comparative assessment results, the proposed protection scheme outperforms those reported in some earlier studies.

5) The feasibility of the practical implementation of the proposed protection scheme is evaluated on the OPAL-RT manufactured RTDS platform.

The remainder of this paper is organized as follows. The details of the proposed protection scheme are discussed in Section II. Section III presents the results and corresponding discussions. The comparative results are presented in Section IV. Section V explicates the performance validation through the OPAL-RT manufactured RTDS platform. Finally, Section VI concludes this paper.

II. PROPOSED PROTECTION SCHEME

The voltage and current signals at the relay location change with the initiation of a fault in the power distribution network. In this study, the calculated differential power from the superimposed voltage and current signals at the relay location is utilized for fault detection. Once a fault is detected, the signs of the computed differential power of each phase at the end of a particular line are compared to identify the faulted phases. To transform the proposed scheme into a threshold-free FPI one, instead of directly utilizing the differential power, a power coefficient index is derived for each phase. The computation steps of the proposed protection scheme are as follows.

The work flow and practical implementation of the proposed protection scheme are shown in Fig. 1. To explain the proposed protection scheme, we take the line 1-2 in Fig. 1 as an example.
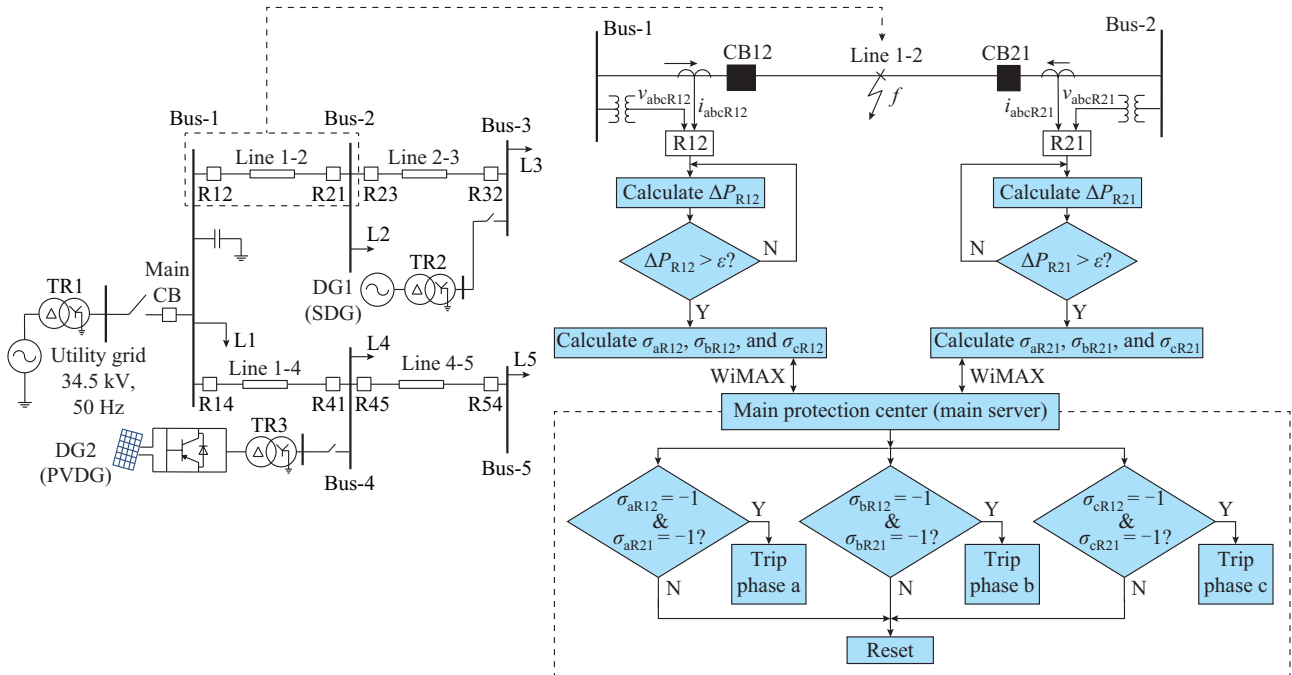

Fig. 1.   Work flow of proposed protection scheme.

The measured voltage and current signals at relay R12 are sampled at 1 kHz, which are denoted as $v_{aR12}(n)$, $v_{bR12}(n)$, $v_{cR12}(n)$ for voltage signals and $i_{aR12}(n)$, $i_{bR12}(n)$, $i_{cR12}(n)$ for current signals at the nth instant, respectively. The one-cycle differences of the voltage and current signals extracted at the nth instant at relay R12 are calculated using (1) and (2), re-

spectively.

$$\begin{cases} \Delta v_{aR12}(n) = v_{aR12}(n) - v_{aR12}(n-N) \\ \Delta v_{bR12}(n) = v_{bR12}(n) - v_{bR12}(n-N) \\ \Delta v_{cR12}(n) = v_{cR12}(n) - v_{cR12}(n-N) \end{cases} \quad (1)$$

$$\begin{cases} \Delta i_{aR12}(n) = i_{aR12}(n) - i_{aR12}(n-N) \\ \Delta i_{bR12}(n) = i_{bR12}(n) - i_{bR12}(n-N) \\ \Delta i_{cR12}(n) = i_{cR12}(n) - i_{cR12}(n-N) \end{cases} \quad (2)$$

where $N = 20$ is the number of samples in one cycle. Similarly, the one-cycle difference of the voltage and current signals can be extracted at relay R21 using (1) and (2). The three-phase voltages and currents at relay R21 at the nth instant are denoted as $v_{aR21}(n)$, $v_{bR21}(n)$, $v_{cR21}(n)$ and $i_{aR21}(n)$, $i_{bR21}(n)$, $i_{cR21}(n)$, respectively. The corresponding one-cycle differences are denoted as $\Delta v_{aR21}(n)$, $\Delta v_{bR21}(n)$, $\Delta v_{cR21}(n)$ and $\Delta i_{aR21}(n)$, $\Delta i_{bR21}(n)$, $\Delta i_{cR21}(n)$, respectively.

The one-cycle differences of voltage and current signals (superimposed components) are conventionally used to detect and classify faults in power transmission and distribution networks [28]. However, the performance of the conventional superimposed approach is affected by the connection of PVDG in the MG [16]. To avoid this, a differential power based scheme is introduced in this study. The superimposed voltage and current components derived from (1) and (2), respectively, are used to calculate the differential power. The differential power magnitudes of the three phases calculated at relays R12 and R21 at the nth instant are expressed in (3) and (4), respectively.

$$\begin{cases} \Delta P_{aR12}(n) = \Delta v_{aR12}(n) \Delta i_{aR12}(n) \\ \Delta P_{bR12}(n) = \Delta v_{bR12}(n) \Delta i_{bR12}(n) \\ \Delta P_{cR12}(n) = \Delta v_{cR12}(n) \Delta i_{cR12}(n) \end{cases} \quad (3)$$

$$\begin{cases} \Delta P_{aR21}(n) = \Delta v_{aR21}(n) \Delta i_{aR21}(n) \\ \Delta P_{bR21}(n) = \Delta v_{bR21}(n) \Delta i_{bR21}(n) \\ \Delta P_{cR21}(n) = \Delta v_{cR21}(n) \Delta i_{cR12}(n) \end{cases} \quad (4)$$

Once the differential power magnitudes of the three phases at relays R12 and R21 are computed, the magnitudes of the three-phase differential power, ΔP_{R12} and ΔP_{R21}, at relays R12 and R21 can be calculated using (5) and (6), respectively.

$$\Delta P_{R12} = \left| \sum \left(\Delta P_{aR12}(n) + \Delta P_{bR12}(n) + \Delta P_{cR12}(n) \right) \right| \quad (5)$$

$$\Delta P_{R21} = \left| \sum \left(\Delta P_{aR21}(n) + \Delta P_{bR21}(n) + \Delta P_{cR21}(n) \right) \right| \quad (6)$$

In this study, ΔP_{R12} and ΔP_{R21} are used as the criteria for the detection of faults in MGs.

Relays R12 and R21 detect a fault if (7) and (8) are satisfied, respectively.

$$\Delta P_{R12} > \varepsilon \quad (7)$$

$$\Delta P_{R21} > \varepsilon \quad (8)$$

where ε is the threshold.

Ideally, the magnitudes of the differential power calculated at relays R12 and R21 are zero during the normal operation of the power system. When a fault initiates, the magni-

tude of the differential power calculated at the relay location increases. Thus, the computed differential power at the relay location can be used as a feature for fault detection. However, during the initiation of non-fault transients, a certain magnitude of differential power exists, which may be misinterpreted as a fault. Thus, a threshold of $\varepsilon = 0.1$ is considered to avoid false fault detection during different non-fault transients. Based on the simulated results, the chosen threshold ε can ensure the reliable fault detection in MGs.

Once a fault is detected, the next task is the FPI. At the relay position, the phasor relationships between the estimated superimposed voltage and current signals of a particular phase during forward and reverse faults are shown in Fig. 2(a) and (b), respectively [29], where Z_s and Z_L are the source and line impedances, respectively. Figure 2 shows that the superimposed voltage and current signals during reverse and forward faults have the same and opposite signs, respectively. Herein, this distinction is utilized for the FPI.
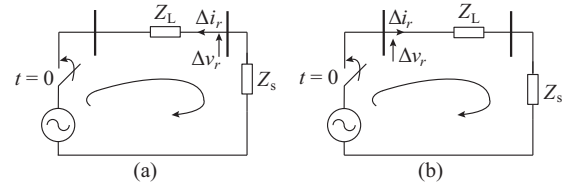

Fig. 2. Relationship between superimposed voltage and current signals extracted during forward and reverse faults. (a) Forward fault. (b) Reverse fault.

Ideally, the calculated line-end differential power of each phase is zero during the normal operation, and after an internal fault occurs, the differential power across the faulted phase becomes negative. However, the simulation study indicates that even during non-fault transients, the differential power values calculated at the line-end phases become negative and have a small magnitude. Thus, for secure discrimination of faults from transients, a suitable threshold is essential. It is further observed that the selection of a suitable threshold for discriminating critical faults (e.g., HIFs) from non-fault transients may become exigent. Moreover, the integration of MGs into distribution systems through power electronic converters affects the voltage and current signals of non-fault phases. In such situations, the proper threshold selection becomes difficult. To solve this problem and make the proposed FPI task threshold-free, the power coefficients σ of individual phases at the line end are calculated; the power coefficient is simply a representation of the differential power per unit. The steps involved in calculating the power coefficients of each phase at the line end and the proposed FPI rules are expressed as:

$$\begin{cases} \sigma_{aR12}(n) = \dfrac{\Delta P_{aR12}(n)}{\max\left(\left| \Delta P_{aR12}(n) \right|, \left| \Delta P_{bR12}(n) \right|, \left| \Delta P_{cR12}(n) \right| \right)} \\[4mm] \sigma_{bR12}(n) = \dfrac{\Delta P_{bR12}(n)}{\max\left(\left| \Delta P_{aR12}(n) \right|, \left| \Delta P_{bR12}(n) \right|, \left| \Delta P_{cR12}(n) \right| \right)} \\[4mm] \sigma_{cR12}(n) = \dfrac{\Delta P_{cR12}(n)}{\max\left(\left| \Delta P_{aR12}(n) \right|, \left| \Delta P_{bR12}(n) \right|, \left| \Delta P_{cR12}(n) \right| \right)} \end{cases} \quad (9)$$

$$\begin{cases} \sigma_{aR21}(n) = \dfrac{\Delta P_{aR21}(n)}{\max\left(\left|\Delta P_{aR21}(n)\right|, \left|\Delta P_{bR21}(n)\right|, \left|\Delta P_{cR21}(n)\right|\right)} \\[2ex] \sigma_{bR21}(n) = \dfrac{\Delta P_{bR21}(n)}{\max\left(\left|\Delta P_{aR21}(n)\right|, \left|\Delta P_{bR21}(n)\right|, \left|\Delta P_{cR21}(n)\right|\right)} \\[2ex] \sigma_{cR21}(n) = \dfrac{\Delta P_{cR21}(n)}{\max\left(\left|\Delta P_{aR21}(n)\right|, \left|\Delta P_{bR21}(n)\right|, \left|\Delta P_{cR21}(n)\right|\right)} \end{cases} \quad (10)$$

where $\sigma_{aR12}(n)$, $\sigma_{bR12}(n)$, $\sigma_{cR12}(n)$ and $\sigma_{aR21}(n)$, $\sigma_{bR21}(n)$, $\sigma_{cR21}(n)$ are the power coefficients of the three phases calculated at relays R12 and R21, respectively.

If (11)-(13) are satisfied, respectively, phases a, b, c will be detected as the fault phase, respectively.

$$\sigma_{aR12}(n) = \sigma_{aR21}(n) = -1 \qquad (11)$$

$$\sigma_{bR12}(n) = \sigma_{bR21}(n) = -1 \qquad (12)$$

$$\sigma_{cR12}(n) = \sigma_{cR21}(n) = -1 \qquad (13)$$

Otherwise, the condition is normal.

In Fig. 1, the three-phase differential power is calculated at the relay location using the measured three-phase voltage and current signals. If the calculated differential power satisfies fault detection criteria (7) and (8), the fault detection unit registers a fault. Once the fault is detected, the power coefficients of the individual phases are calculated at their respective relay locations using (9) and (10) and transmitted to the main protection center through the worldwide interoperability for microwave access wireless (WiMAX) communication technology. The power coefficients of the corresponding phases at both ends of a feeder are compared. If any of the FPI criteria (i.e., (11), (12), or (13)) is satisfied, the tripping command is transmitted to the respective feeder relays to isolate the faulted phases. WiMAX is a standard communication protocol that focuses on fixed wireless application with a coverage of up to 50 km and a communication delay of approximately 2 ms [30]. As indicated in the proposed scheme, a communication medium is only used to transmit the signs of the computed power coefficients of the three phases; consequently, signal transmission latency can be expected within 1 ms. Such a fast latency does not affect the speed of the proposed protection scheme.

III. RESULTS AND DISCUSSIONS

The system shown in Fig. 1 is used for data generation, where DG1 and DG2 are a synchronous distributed generator (SDG) and an inverter-interfaced PVDG with capacities of 20 MVA and 10 MW, respectively. Figure 1 also shows that the SDG and PVDG are connected to the power grid at Bus-3 and Bus-4, respectively. The control scheme for the integration of the PVDG to the main grid is modelled as that in [16]. There are five loads (L1-L5) in the system, and the line and load data are similar to those in [16]. The DG devices are integrated as per IEEE 1547 [31]. Various faults and non-fault transients generated in different MG operation modes through the PSCAD/EMTDC for the performance assessment of the proposed protection scheme are summarized in Table I. A total of 11100 test cases are generated for the performance evaluation of the proposed protection scheme.

Some of the important results from each category are discussed below.

TABLE I
LIST OF DIFFERENT SIMULATED CASES

Case	System operation condition
Operation mode	Grid-connected and islanding modes (2 cases)
DG type	PVDG and SDG (2 cases)
Load type	Balanced and unbalanced loads (2 cases)
Fault type	Line-to-ground (AG, BG, CG), line-to-line (AB, BC, CA), double-line-to-ground (ABG, BCG, CAG), three-phase (ABC, ABCG), and HIFs with low-arcing currents (11 cases)
Fault inception angle	0°, 45°, 90°, 135°, and 180° (5 cases)
Fault resistance	1 Ω, 10 Ω, 25 Ω, 50 Ω, and 100 Ω (5 cases)
Fault location	At 25%, 50%, 70%, 80%, and 90% length of different feeders (5 cases)
Non-fault transient	Large load switching, capacitor switching, DG outage, line outage, and presence of noise in measured current signal, etc. (total 100 cases)
Total test cases generated	$2 \times 2 \times 2 \times 11 \times 5 \times 5 \times 5 + 100 = 11000 + 100 = 11100$

A. Faults Occurring in Grid-connected Mode (Only SDG is Grid-connected)

1) Results of Single-phase-to-ground Fault

An AG fault (fault resistance $R_f = 10\ \Omega$) is set in line 1-2 at 2.2 s with 4 km from relay R12 (Fig. 1). The three-phase currents and voltages measured by relays R12 and R21 at both ends of line 1-2 are shown in Fig. 3(a) and (b), respectively. Immediately after the fault is initiated at 2.2 s, the magnitudes of differential power computed at relays R12 and R21, ΔP_{R12} and ΔP_{R21}, increase from zero (Fig. 3(c)), satisfying the fault detection criteria in 2 ms. Further, to ascertain the fault phases, the power coefficients of the three phases at the ends of line 1-2 are calculated and presented in Fig. 3(d). The power coefficients of phase a at the ends of line 1-2 satisfy (11), and the proposed FPI algorithm detects the fault phase a in only 2 ms (Fig. 3(e)).

The results of the adjacent non-fault line 2-3, as shown in Fig. 4, can be used to check the security aspect of the proposed FPI algorithm. Since the SDG is the downstream of lines 1-2 and 2-3, the current and voltage patterns at the ends of lines 2-3 and 1-2, resulting from a fault in line 1-2, are similar. Thus, although the fault is in line 1-2, the fault detection criteria at the ends of lines 2-3 are also satisfied (Fig. 4(c)). However, the FPI criteria are not satisfied for any of the phases of line 2-3 (Fig. 4(d)). Thus, a fault in line 1-2 is treated by the end relays of line 2-3 as an external fault.

2) Results of Double-phase Fault

An AC fault is set in line 2-3 at 2.3 s with 5 km from relay R23 (Fig. 1). The corresponding results are shown in Fig. 5. In this case and at the inception of the AC fault, the calculated magnitudes of differential power at relays R23 and R32 increase from zero, and the fault is detected in 2 ms (Fig. 5(c)). The power coefficient based algorithm clearly shows that the FPI criteria of only phase a and phase c are satisfied and correctly detected in only 2 ms (Fig. 5(e)).
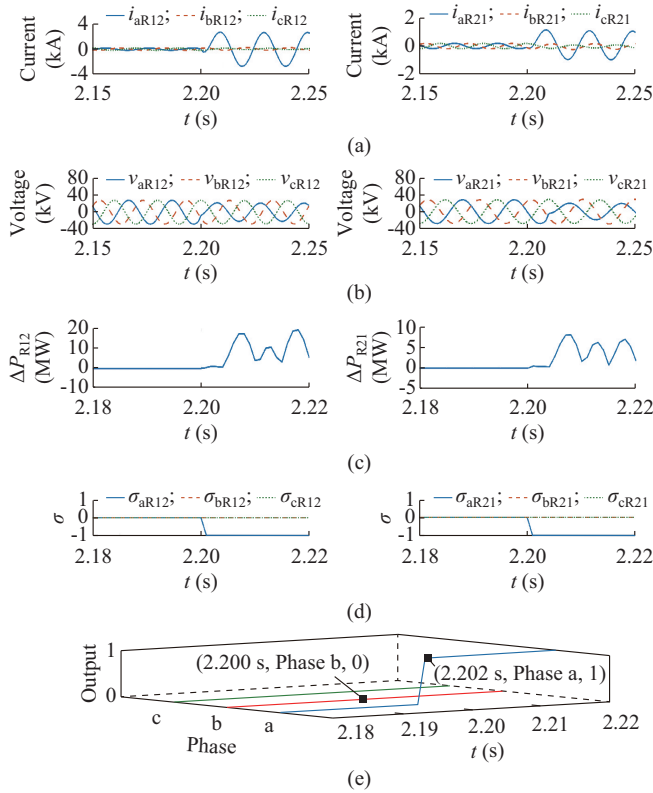
Fig. 3. Performance results at relays R12 and R21 during AG fault in line 1-2. (a) Current. (b) Voltage. (c) Differential power ΔP. (d) Power coefficient σ. (e) Output.
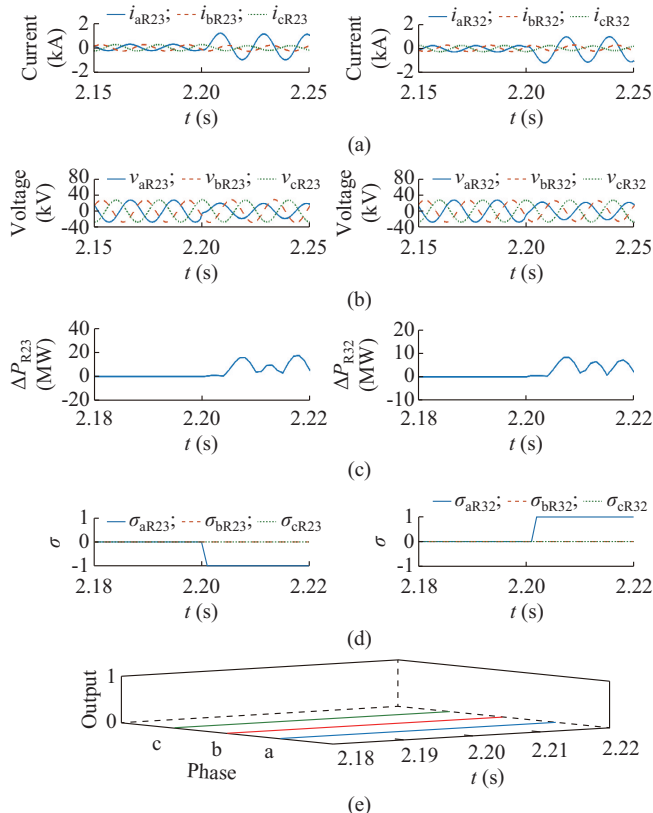

Fig. 4. Performance results at relays R23 and R32 during AG fault in line 1-2. (a) Current. (b) Voltage. (c) Differential power ΔP. (d) Power coefficient σ. (e) Output.
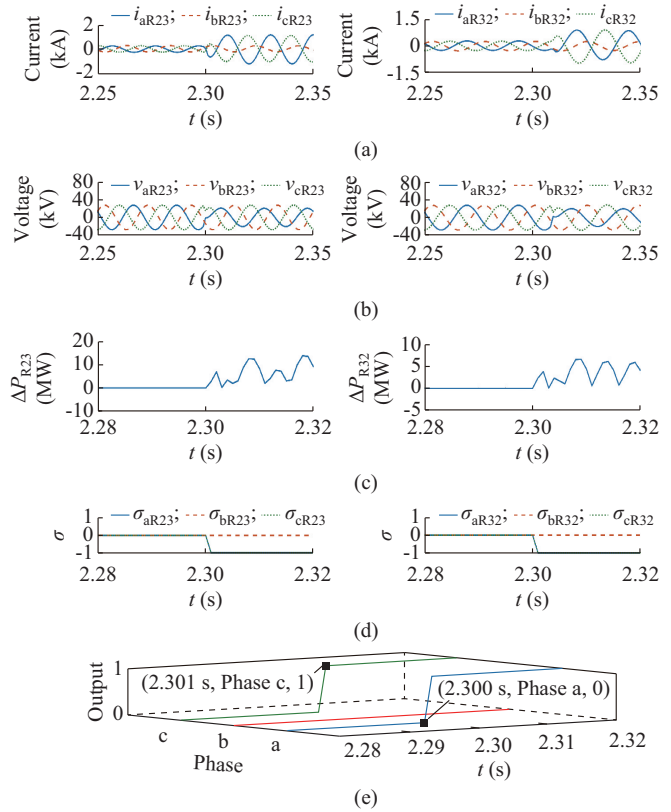

Fig. 5. Performance results at relays R23 and R32 during AC fault in line 2-3. (a) Current. (b) Voltage. (c) Differential power ΔP. (d) Power coefficient σ. (e) Output.

Further, an ABG fault ($R_f = 10$ Ω) is set in line 2-3 at 2.5 s with 3 km from relay R23. The results in Fig. 6 show that the differential power based fault detection and power coefficient based FPI criteria are satisfied at the ends of line 2-3. The proposed protection scheme detects the fault phases in only 2 ms (Fig. 6(e)).

3) Results of High-resistance Ground Fault

A high-resistance BG fault ($R_f = 50$ Ω) is set in line 1-2 at 2.4 s with 6 km from relay R12 (Fig. 1). Figure 7 clearly shows that due to the high fault resistance, the change in the current magnitude from the normal operation to the fault is insignificant. Despite this, the calculated magnitudes of differential power at relays R12 and R21 satisfy the fault detection criteria (Fig. 7(c)). Further, Fig. 7(d) shows that only the FPI criteria of phase b in line 1-2 are satisfied and detected in only 1 ms (Fig. 7(e)).

4) Results of HIF

In electric power distribution systems, energized conductors usually meet poorly grounded objects such as trees, wood fences, and vehicles. Sometimes, the overhead conductors break and touch high-impedance ground surfaces such as asphalt, concrete, grass, and sand. These contacts restrict the fault current from a few milliamperes to 75 A only [32]. Such HIFs with low-arcing currents are not effectively detected by overcurrent relays. Although they cause no damage to the power distribution network components, the energized conductors on the ground surface can pose a threat to human life. In addition, arcing caused by such faults are fire hazards.
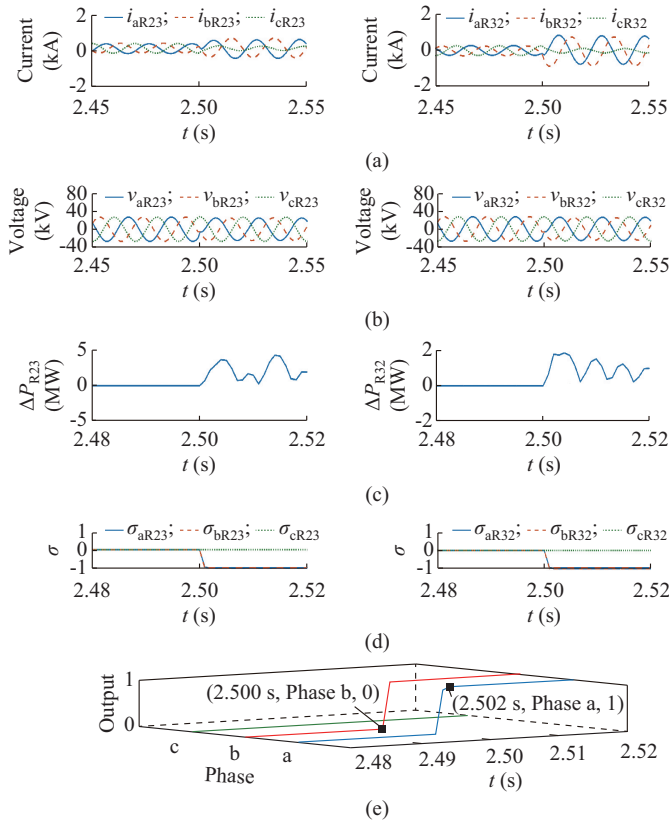
Fig. 6. Performance results at relays R23 and R32 during ABG fault in line 2-3. (a) Current. (b) Voltage. (c) Differential power ΔP. (d) Power coefficient σ. (e) Output.
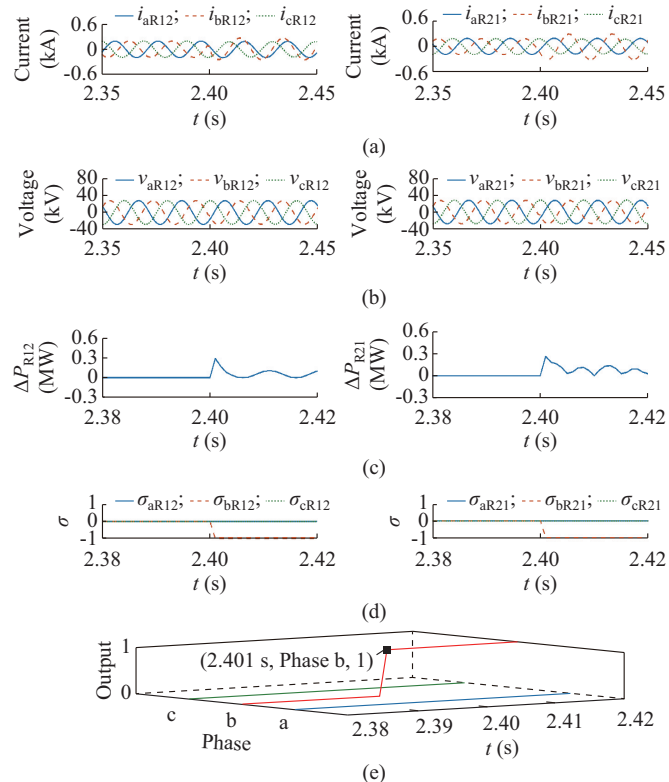

Fig. 7. Performance results at relays R12 and R21 during high-resistance BG fault in line 1-2. (a) Current. (b) Voltage. (c) Differential power ΔP. (d) Power coefficient σ. (e) Output.

Thus, it is necessary to correctly detect HIFs in electric power distribution networks. However, HIF detection becomes more difficult with the increasing penetration of renewable energy based DGs into the distribution networks [33].

The HIF currents are associated with electric arcs and hence are random, non-linear, asymmetric, and intermittent. The circuit model considered in this study, exhibiting the above characteristics of the HIF current, is similar to that in [32] and is reproduced in Fig. 8. In Fig. 8, one path consists of a DC voltage source V_p, a diode D_p, and a variable resistor R_p; similarly, the other path consists of V_q, D_q, and R_q. This HIF model is connected to the middle of phase a in line 1-2 shown in Fig. 1 and short-circuited to the ground at 2.5 s. The voltage and current waveforms at the HIF location are shown in Fig. 9, which indicate the nonlinearity and randomness of the HIF. In addition, the HIF current magnitude is restricted to less than 75 A. The results of the fault case are shown in Fig. 10. The differential power and power coefficient criteria are satisfied, and the FPI criteria are satisfied and correctly detected in 7 ms (Fig. 10(d)). This shows that the proposed protection scheme is highly sensitive even to HIFs with low-arcing currents.
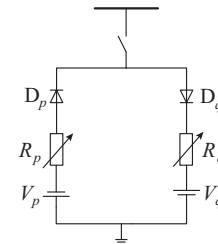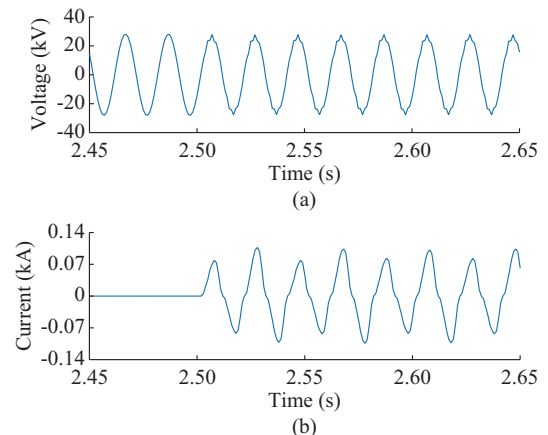

Fig. 8. Schematic diagram of HIF model.

Fig. 9. Typical voltage and current waveforms during HIF. (a) Voltage. (b) Current.

B. Faults Occurring in Grid-connected Mode (Only PVDG is Grid-connected)

1) Results of Single-phase-to-ground Fault

A CG fault ($R_f = 50\ \Omega$) is created in line 1-4 at 3.2 s with 7 km from relay R14 (Fig. 1). The corresponding results of the fault case are shown in Fig. 11. As shown in Fig. 11(a), the currents of the non-fault phases, especially near relay R41, i.e., close to the PVDG, are also affected. Despite this,

the calculated differential power (Fig. 11(c)) and the power coefficients (Fig. 11(d)) at both ends of line 1-4 satisfy the corresponding detection criteria, and the proposed scheme detects the fault phase (phase c) in only 1 ms (Fig. 11(e)).
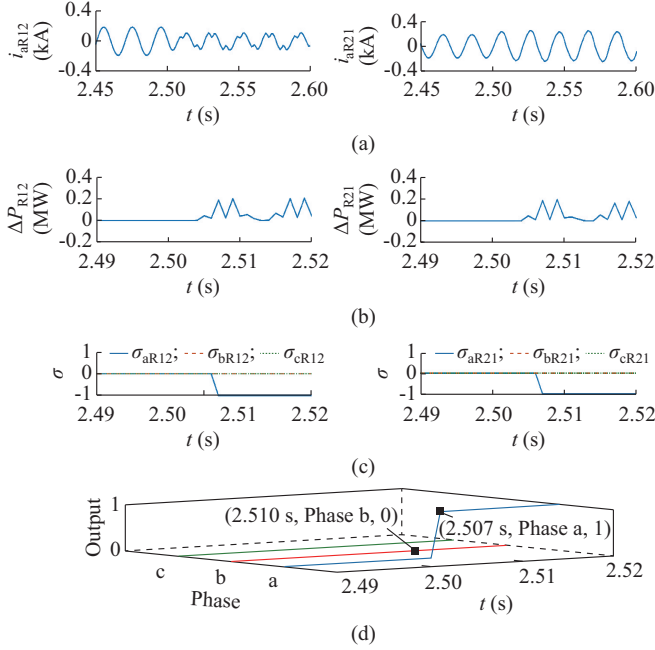

Fig. 10. Performance results at relays R12 and R21 during HIF (AG type) in line 1-2. (a) Current. (b) Differential power ΔP. (c) Power coefficient σ. (d) Output.
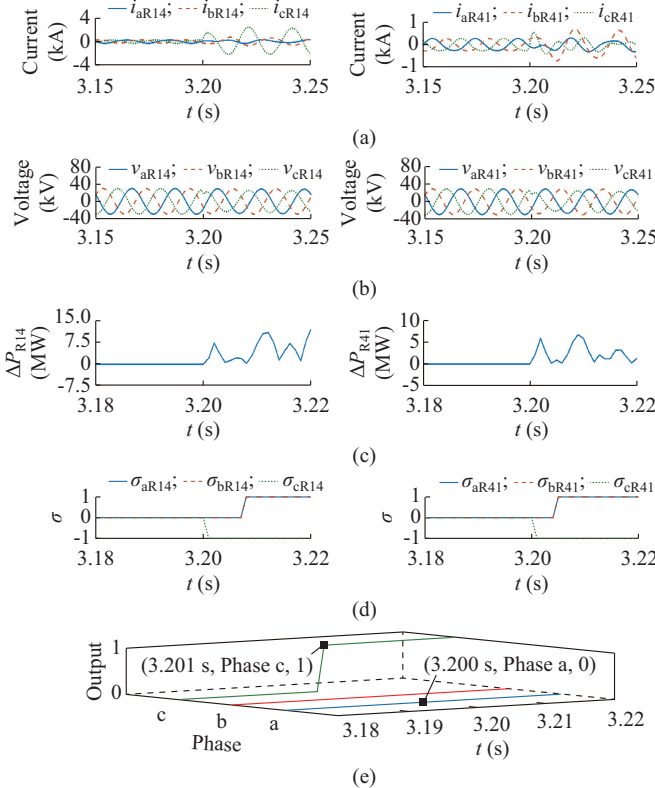

Fig. 11. Performance results at relays R14 and R41 during CG fault in line 1-4. (a) Current. (b) Voltage. (c) Differential power ΔP. (c) Power coefficient σ. (e) Output.

2) Results of Double-phase-to-ground Fault

A BCG fault ($R_f = 10\ \Omega$) is initiated in line 1-4 at 2.7 s with 8 km from relay R14 (Fig. 1). The corresponding results are shown in Fig. 12. As shown in Fig. 12(e), the FPI task is performed in only 3 ms.
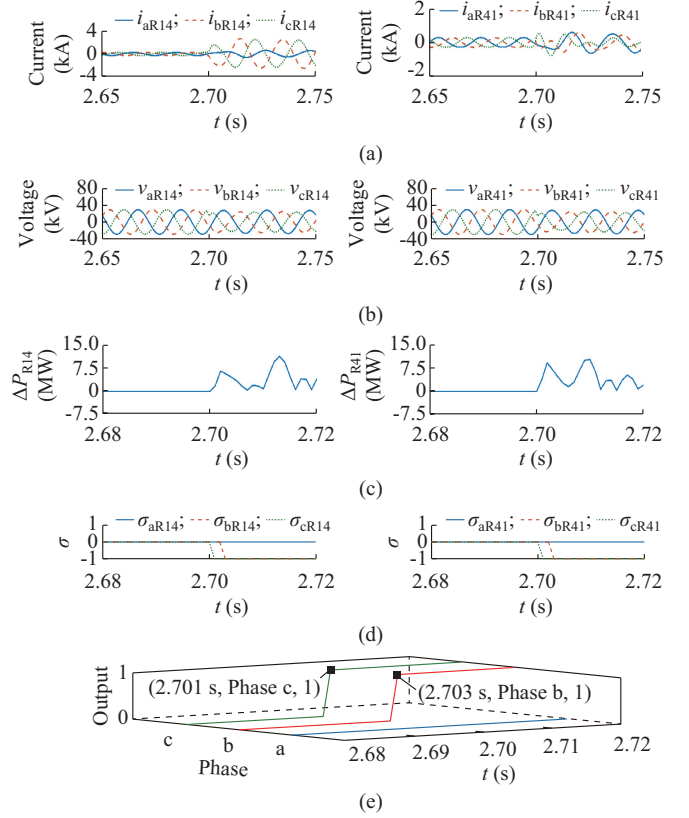

Fig. 12. Performance results at relays R14 and R41 during BCG fault in line 1-4. (a) Current. (b) Voltage. (c) Differential power ΔP. (c) Power coefficient σ. (e) Output.

C. Faults Occurring in Islanding Mode (Grid is Disconnected)

1) Results of Single-phase-to-ground Fault

In the islanding mode, an AG fault ($R_f = 10\ \Omega$) is initiated in line 2-3 at 3.1 s with 3 km from relay R23 (Fig. 1). The corresponding results are shown in Fig. 13. In Fig. 13(a), the currents of non-fault phases are also affected by the presence of power from the inverter-interfaced PVDG. Despite the irregular patterns of currents in the non-fault phases, the proposed scheme performs the FPI task in only 1 ms (Fig. 13(e)). Thus, the performance of the present scheme is independent of the operation modes of MG.

2) Results of Single-phase Fault During Unbalanced Loading

Distribution networks sometimes operate with unbalanced loads. In the islanding mode, let phase c of load L5 be disconnected, which results in an unbalanced condition in the system. During this period, a BG fault ($R_f = 20\ \Omega$) is initiated in line 4-5 at 2.3 s with 6 km from relay R45 (Fig. 1). The corresponding results are presented in Fig. 14. Under the unbalanced load condition, the initiation of the BG fault causes ΔP and σ of phase b to satisfy their preset thresholds, and the proposed scheme detects the fault phase (phase b) in only 2 ms (Fig. 14(e)).
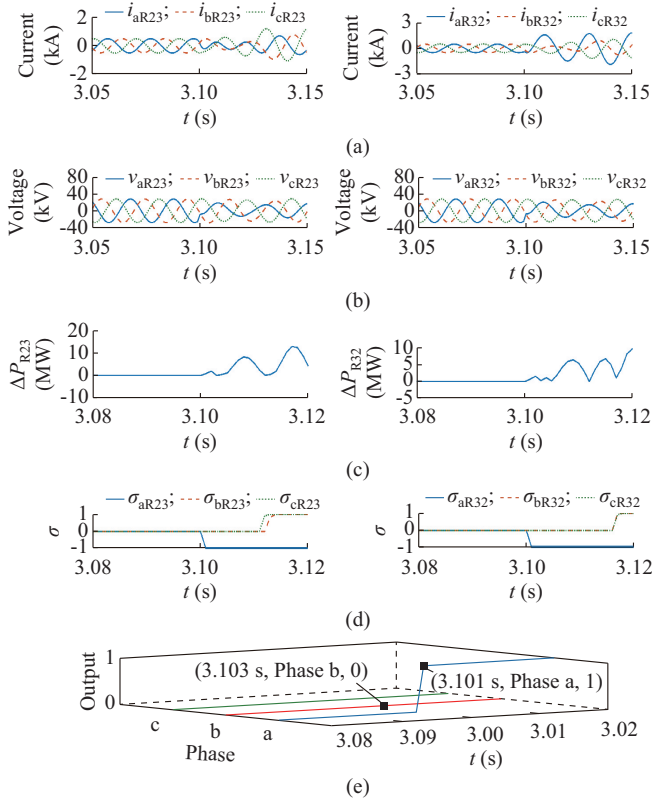
Fig. 13.   Performance results at relays R23 and R32 during AG fault in line 2-3. (a) Current. (b) Voltage. (c) Differential power ΔP. (c) Power coefficient σ. (e) Output.
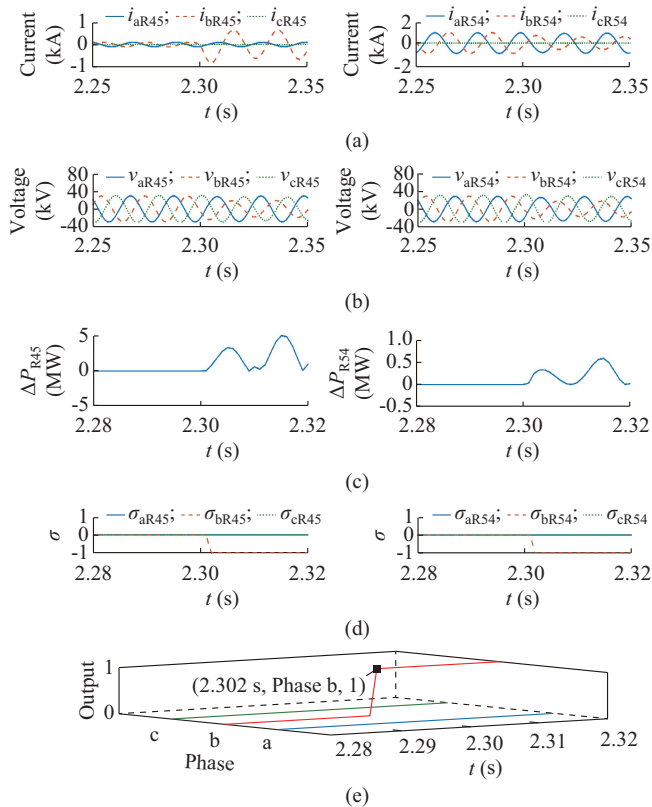

Fig. 14.   Performance results at relays R45 and R54 during BG fault with unbalanced load in line 4-5. (a) Current. (b) Voltage. (c) Differential power ΔP. (c) Power coefficient σ. (e) Output.

3) Results of Double-phase-to-ground Fault

In the islanding mode, an ABG fault ($R_f = 10$ Ω) is initiated in line 1-2 at 3.4 s with 7 km from relay R12 (Fig. 1). The corresponding results are shown in Fig. 15. As shown in Fig. 15(e), the FPI criteria are satisfied at the ends of line 1-2, and the fault phases (phase a and phase b) are identified in only 1 ms.
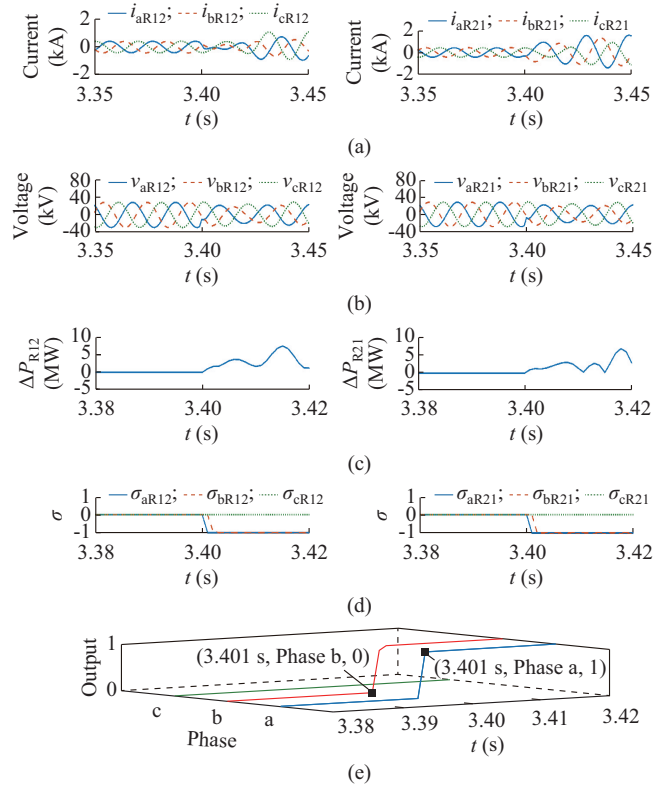

Fig. 15.   Performance results at relays R12 and R21 during ABG fault in line 1-2. (a) Current. (b) Voltage. (c) Differential power ΔP. (c) Power coefficient σ. (e) Output.

D. Robustness to Non-fault Transients in MGs

For security assessment, the proposed protection scheme is tested on different possible switching events such as large load switching, capacitor switching, sudden DG outages, line outages, and presence of noise in the current signal. The corresponding results of some non-fault transient cases are considered below.

1) Results of Large Load Switching

At 3.5 s, load L2 at Bus-1 suddenly increases to 1.4 times the rated value (Fig. 1). The effects of load switching on Bus-1 at both ends of the relays of adjacent lines (lines 1-2 and 2-3) are evaluated. However, owing to page restrictions, only the results of line 1-2 are provided in Fig. 16. As shown in Fig. 16(c) and (d), none of the fault detection and isolation criteria at the ends of lines 1-2 is satisfied, and the algorithm is not activated. Thus, load switching is not a problem for the proposed protection scheme.

2) Results of Capacitor Switching

A 1.5 kvar capacitor connected to Bus-1 (Fig. 1) is suddenly switched off at 3.0 s. The effects of capacitor switching on Bus-1 at both ends of the relays of adjacent lines

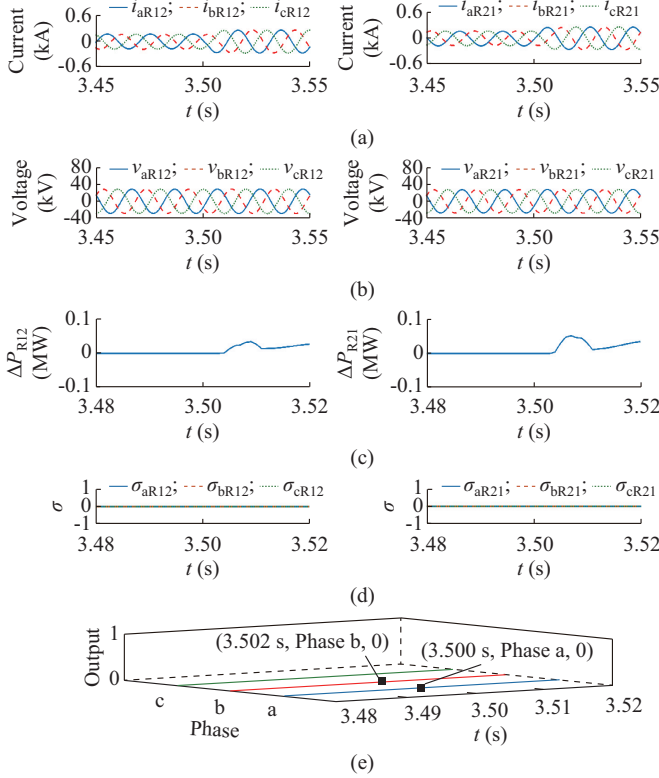(lines 1-2 and 2-3) are evaluated. For simplification, only the results of line 2-3 are presented in Fig. 17.

Fig. 16. Performance results at relays R12 and R21 during load switching at Bus-1. (a) Current. (b) Voltage. (c) Differential power ΔP. (c) Power coefficient σ. (e) Output.

As shown in Fig. 17(c), the calculated magnitudes of differential power at both ends of line 2-3 exceed their respective thresholds. Thus, capacitor switching is detected as a fault event, activating the FPI algorithm. However, as shown in Fig. 17(d), the calculated power coefficients at both ends of line 2-3 have opposite signs, confirming that capacitor switching is a non-fault event (Fig. 17(e)).

3) Results of DG Outage

The PVDG is suddenly disconnected at 2.1 s from the utility grid (Fig. 1), and the test results of line 1-4 are provided in Fig. 18. The changes of the voltage and current signals due to the sudden outage of PVDG satisfy the differential power based fault detection criteria (Fig. 18(c)). However, the power coefficients at both ends of the three phases have opposite signs, confirming that the DG outage is a non-fault event.

IV. COMPARATIVE ASSESSMENT

The proposed relay scheme is compared with three recent relay schemes proposed for MG protection, namely S-transform operated differential energy scheme [20], cross-alienation coefficient scheme [17], and a scheme based on the active power of zero- or d-frame component consumed by fault resistance [21]. A performance comparison between two critical fault modes is provided below.
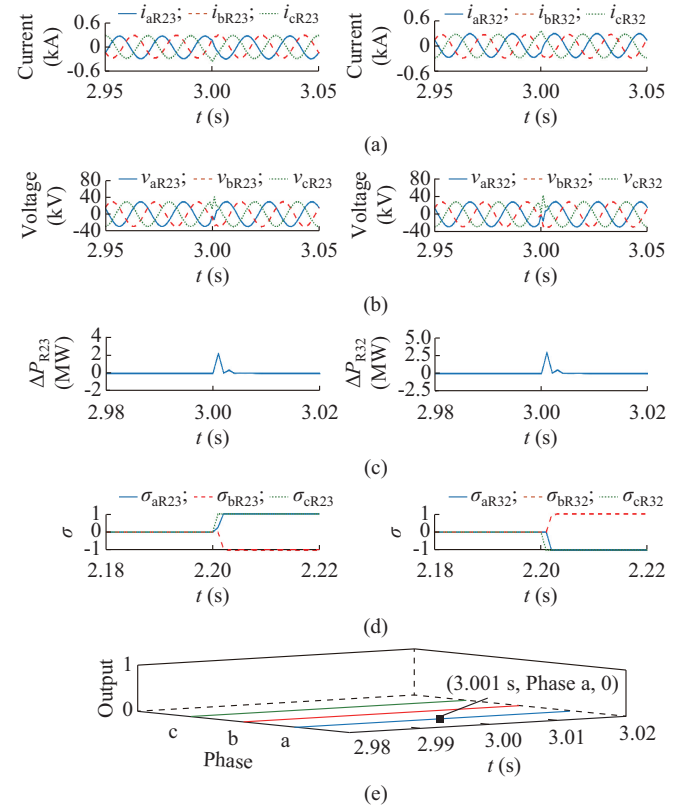

Fig. 17. Performance results at relays R23 and R32 during capacitor switching at Bus-1. (a) Current. (b) Voltage. (c) Differential power ΔP. (c) Power coefficient σ. (e) Output.
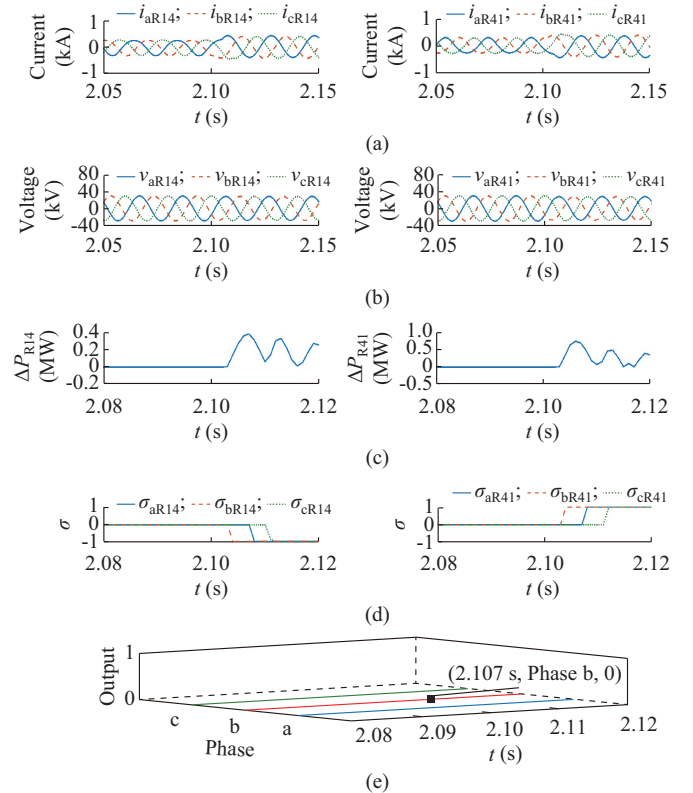

Fig. 18. Performance results at relays R14 and R41 during sudden outage of PVDG at Bus-4. (a) Current. (b) Voltage. (c) Differential power ΔP. (c) Power coefficient σ. (e) Output.

A. Comparative Results of High-resistance Fault in Islanding Mode

The comparative results of a high-resistance CG fault ($R_f =$ 100 Ω) initiated at 3.7 s with 7 km from relay R14 in line 1-4 (Fig. 1) in the islanding mode are presented in Fig. 19.
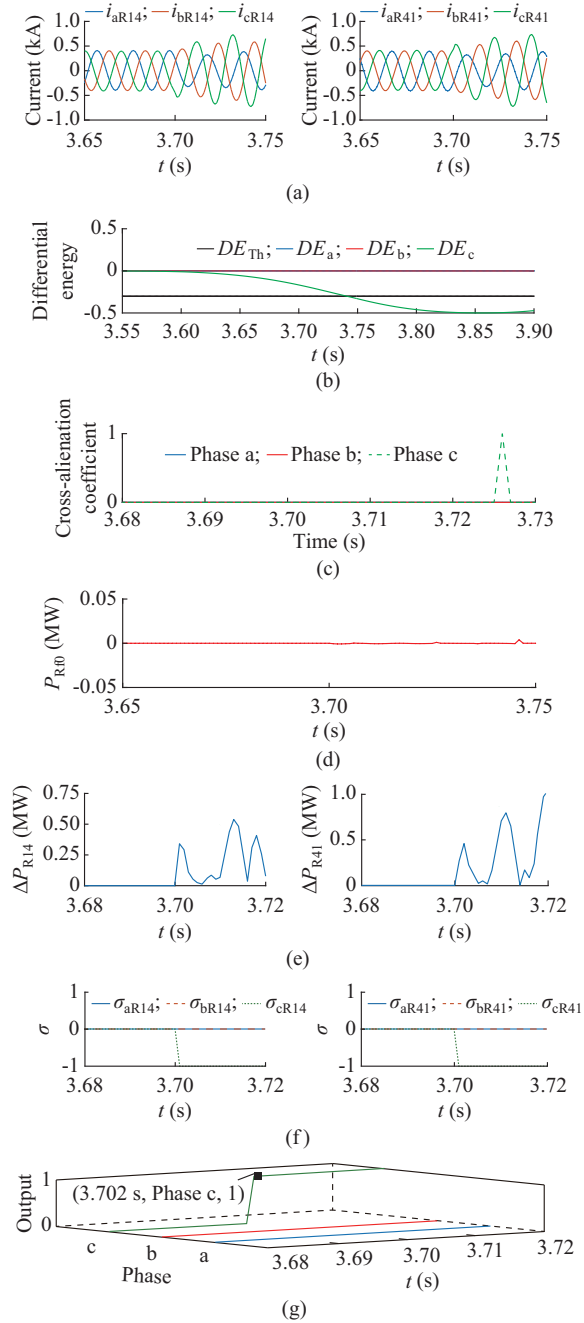

Fig. 19. Comparative assessment results during high-resistance CG fault in line 1-4. (a) Currents measured at relays R14 and R41. (b) S-transform operated differential energy scheme. (c) Cross-alienation coefficient method. (d) Active power of zero- or *d*-frame component consumed by fault resistance ΔP_{Rf0}. (e) Differential power ΔP. (f) Power coefficient σ. (g) Output.

As shown in Fig. 19(b), the S-transform operated differential energy of phase c DE_c exceeds the preset threshold DE_{Th}. Moreover, this scheme can detect the high-resistance fault but requires 41 ms. Similarly, Fig. 19(c) indicates that the cross-alienation coefficient scheme can detect phase c as

the fault phase but requires 26 ms. Further, Fig. 19(d) shows that the scheme based on the active power of zero- or *d*-frame component consumed by fault resistance is unable to detect high-resistance ground faults in MGs. By contrast, the proposed scheme can detect the fault phase (phase c) in only 2 ms (Fig. 19(e)-(g)).

B. Comparative Results of HIF in Grid-connected Mode

The comparative results of an HIF (AG type) in line 1-2 with 8 km from relay R12 (Fig. 1) in the grid-connected mode (only the SDG is connected to the power grid) are shown in Fig. 20.

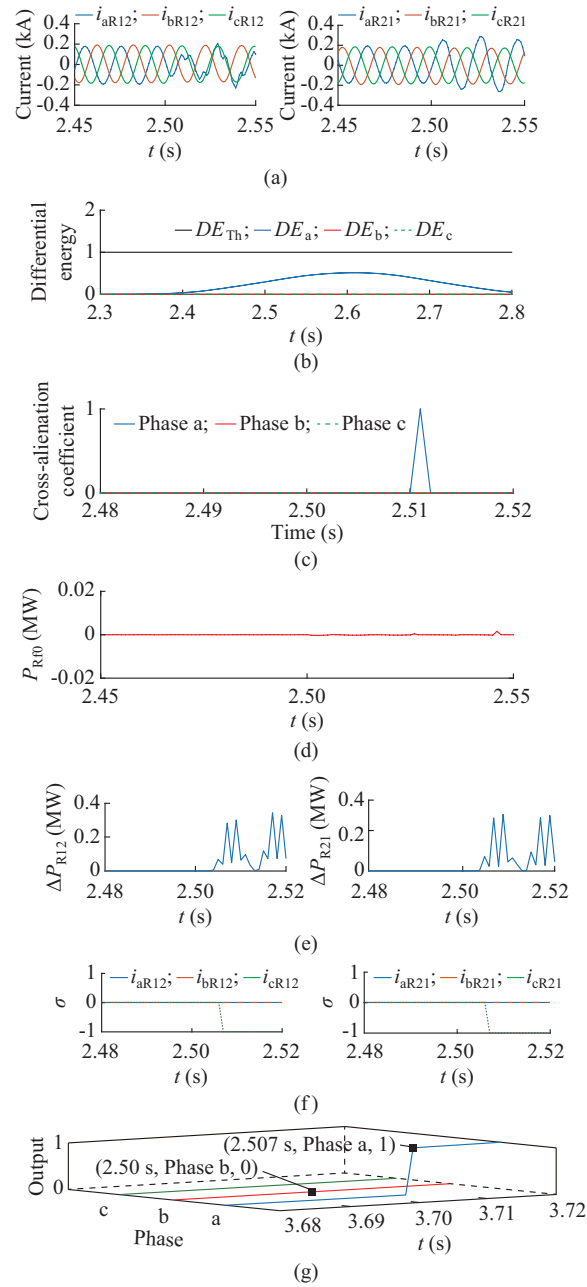
Fig. 20. Comparative assessment results during HIF (AG type) in line 1-2. (a) Currents measured at relays R12 and R21. (b) S-transform operated differential energy scheme. (c) Cross-alienation coefficient scheme. (d) Active power of zero- or *d*-frame component consumed by fault resistance ΔP_{Rf0}. (e) Differential power ΔP. (f) Power coefficient σ. (g) Output.

The HIF model shown in Fig. 8 is used for the present comparative study. As shown in Fig. 20(b), the S-transform operated differential energy scheme is unable to detect the HIF as the derived feature of phase a, i.e., DE_a is less than its preset threshold DE_{Th}. However, the cross-alienation coefficient scheme can detect the HIF (AG type) in 12 ms (Fig. 20(c)). Further, the scheme based on the active power of zero- or d-frame component consumed by fault resistance is unable to detect the HIF (Fig. 20(d)). By contrast, the proposed scheme can detect the HIF (AG type) in only 7 ms (Fig. 20(e)-(g)).

The comparative results of these two fault modes confirm that the proposed scheme can detect even the critical faults in MGs and isolate them more quickly and securely than others. Thus, the proposed relay scheme outperforms those reported in some earlier studies in detecting and isolating fault phases in MGs.

V. PERFORMANCE VALIDATION THROUGH RTDS PLATFORM

To evaluate the effectiveness and correctness of the proposed selective phase tripping scheme in a real network, it is implemented and validated through the OPAL-RT manufactured (OP4510) RTDS platform. The hardware setup for the real-time simulation study is shown in Supplement Materials. For simplification, the result of only one fault case is presented.

An AG fault ($R_f = 10\ \Omega$) is initiated in line 1-2 at 2.5 s with 7 km from relay R12 (Fig. 1) in the grid-connected mode. The current and voltage signals measured at relays R12 and R21 are shown in Fig. 21(a) and (b), respectively. The output of the proposed FPI scheme is shown in Fig. 21(c). The fault phase (phase a) is detected in only 3 ms, indicating that the result obtained through the RTDS platform is the same as those previously obtained using the PSCAD/ EMTDC simulation software. Thus, the proposed relay scheme can be facilely implemented for the practical protection of MGs.

VI. CONCLUSION

In this study, a differential power coefficient based threshold-free and computationally efficient protection scheme is proposed for the selective tripping of fault phases in modern MGs consisting of PVDGs and SDGs. The performance of the proposed protection scheme is validated on numerous faults, including critical faults (high-resistance faults and HIFs with low-arcing currents) and non-fault transients (large load switching, capacitor switching, DG outage, line outage, etc.) simulated in a standard MG operating in both grid-connected and islanding modes. The results indicate that through the proposed protection scheme, fault phases, including critical faults in MGs, can be detected and isolated within 10 ms (half a cycle of the power frequency signal). In addition, the scheme is immune to switching transients. Comparative assessment results also clearly show that the proposed protection scheme outperforms the available protection techniques, especially in the detection and isolation of critical faults such as high-resistance faults and low-current

arcing HIFs in MGs. Further, the RTDS results through OPAL-RT (OP4510) prove the feasibility of the proposed protection scheme for its practical implementation as MG protection.
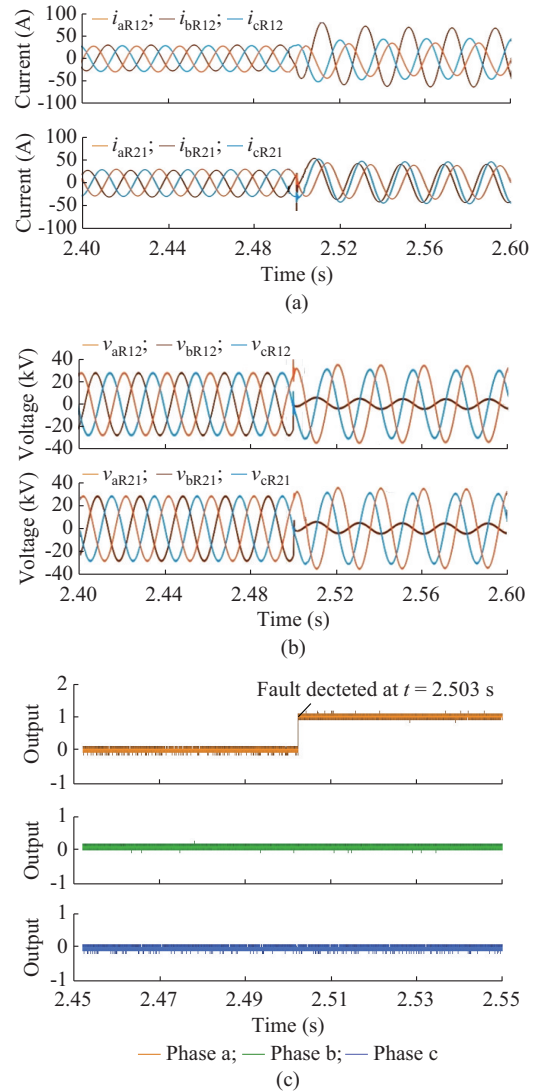

Fig. 21. RTDS results at relays R12 and R21 during AG fault in line 1-2 in grid-connected mode. (a) Current. (b) Voltage. (c) Output.

REFERENCES

[1] S. Parhizi, H. Lotfi, A. Khodaei *et al.*, "State of the art in research on microgrids: a review," *IEEE Access*, vol. 3, pp. 890-925, Jun. 2015.

[2] R. F. Arritt and R.C. Dugan, "Distribution system analysis and the future smart grid," *IEEE Transactions on Industrial Applications*, vol. 47, no. 6, pp. 2343-2350, Sept. 2011.

[3] A. Girgis and S. Brahma, "Effect of distributed generation on protective device coordination in distribution system," in *Proceedings of International Conference Power Engineering in Large Engineering Systems*, Halifax, Canada, Jul. 2001, pp. 115-119.

[4] L. V. Strezoski, N. R. Vojnovic, V. C. Strezoski *et al.*, "Modeling challenges and potential solutions for integration of emerging DERs in DMS applications: power flow and short-circuit analysis," *Journal of Modern Power Systems and Clean Energy*, vol. 7, no. 6, pp. 1365-1384, Nov. 2019.

[5] T. K. Abdel-Galil, A. E. Abu-Elanien, E. F. El-Saadany *et al.*, "Protection coordination planning with distributed generation," *Qualsys Engineering Company Incorporated*, vol. 149, pp. 98-107, Jun. 2007.

[6] S. A. Gopalan, V. Sreeram, and H. H. C. Iu, "A review of coordination strategies and protection schemes for microgrids," *Renewable and Sustainable Energy Review*, vol. 32, pp. 222-228. Mar. 2014.

[7] P. Mahat, Z. Chen, B. Bak-Jensen *et al*., "A simple adaptive overcurrent protection of distribution systems with distributed generation," *IEEE Transactions on Smart Grid*, vol. 2, no. 3, pp. 428-437, Jun. 2011.

[8] A. Oudalov and A. Fidigatti, "Adaptive network protection in microgrids," *International Journal of Distribution Energy Resources*, vol. 5, no. 3, pp. 201-226, Sept. 2009.

[9] M. S. Elbana, N. Abbasy, A. Meghed *et al*., "μPMU-based smart adaptive protection scheme for microgrids," *Journal of Modern Power Systems and Clean Energy*, vol. 7, no. 4, pp. 887-898, Jun. 2019.

[10] E. Sortomme, S. S. Venkata, and J. Mitra, "Microgrid protection using communication-assisted digital relays," *IEEE Transactions on Power Delivery*, vol. 25, no. 4, pp. 2789-2796, Oct. 2009.

[11] T. S. Ustun, C. Ozansoy, and A. Zayegh, "Modeling of a centralized microgrid protection system and distributed energy resources according to IEC 61850-7-420," *IEEE Transactions on Power Systems*, vol. 27, no. 3, pp. 1560-1567, Feb. 2012.

[12] J. R. Agüero, J. Wang, and J. J. Burke, "Improving the reliability of power distribution systems through single-phase tripping," in *Proceedings of IEEE PES Transmission and Distribution Conference and Exposition*, New Orleans, USA, Apr. 2010, pp. 1-7.

[13] Q. Li, Z. Xu, and L. Yang, "Recent advancements on the development of microgrids," *Journal of Modern Power Systems and Clean Energy*, vol. 2, no. 3, pp. 206-211, Sept. 2014.

[14] A. M. El-Zonkoly, "Fault diagnosis in distribution networks with distributed generation," *Electric Power Systems Research*, vol. 81, no. 7, pp. 1482-1490, Jul. 2011.

[15] M. Dewadasa, A. Ghosh, G. Ledwich *et al*., "Fault isolation in distributed generation connected distribution networks," *IET Generation, Transmission & Distribution*, vol. 5, no. 10, pp. 1053-1061, Oct. 2011.

[16] A. Hooshyar, E. F. El-Saadany, and M. Sanaye-Pasand, "Fault type classification in microgrids including photovoltaic DGs," *IEEE Transactions on Smart Grid*, vol. 7, no. 5, pp. 2218-2229, Sept. 2015.

[17] M. M. Mahfouz and M. A. El-Sayed, "Smart grid fault detection and classification with multi-distributed generation based on current signals approach," *IET Generation, Transmission & Distribution*, vol. 10, no. 16, pp. 4040-4047, Dec. 2016.

[18] O. Dharmapandit, R. K. Patnaik, and P. K. Dash, "Detection, classification, and location of faults on grid-connected and islanded AC microgrid," *International Transactions on Electrical Energy Systems*, vol. 27, no. 12, pp. 1-33, Dec. 2017.

[19] E. Casagrande, W. L. Woon, H. H. Zeineldin *et al*., "A differential sequence component protection scheme for microgrids with inverter-based distributed generators," *IEEE Transactions on Smart Grid*, vol. 5, no. 1, pp. 29-37, Jan. 2014.

[20] S. Kar and S. R. Samantaray, "Time-frequency transform-based differential scheme for microgrid protection," *IET Generation, Transmission & Distribution*, vol. 8, no. 2, pp. 310-320, Feb. 2014.

[21] X. Liu, Z. Xie, Q. Sun *et al*., "A novel protection scheme against fault resistance for AC microgrid," *Mathematical Problems in Engineering*, vol. 2017, pp. 1-11, Feb. 2017.

[22] H. Lala, S. Karmakar, and S. Ganguly, "Detection and localization of faults in smart hybrid distributed generation systems: a Stockwell transform and artificial neural network-based approach," *International Transactions on Electrical Energy Systems*, vol. 29, no. 2, pp. 1-18, Feb. 2019.

[23] S. Kar, S. R. Samantaray, and M. D. Zadeh, "Data-mining model based intelligent differential microgrid protection scheme," *IEEE Systems Journal*, vol. 11, no. 2, pp. 1161-1169, Jan. 2015.

[24] D. P. Mishra, S. R. Samantaray, and G. Joos, "A combined wavelet and data-mining based intelligent protection scheme for microgrid," *IEEE Transactions on Smart Grid*, vol. 7, no. 5, pp. 2295-2303, Oct. 2016.

[25] M. Dehghani, M. H. Khooban, and T. Niknam, "Fast fault detection and classification based on a combination of wavelet singular entropy theory and fuzzy logic in distribution lines in the presence of distributed generations," *International Journal of Electrical Power and Energy Systems*, vol. 78, pp. 455-462, Jun. 2016.

[26] M. Mishra and R. K. Rout, "Detection and classification of micro-grid faults based on HHT and machine learning techniques," *IET Generation, Transmission & Distribution*, vol. 12, no. 2, pp. 388-397. Sept. 2017.

[27] S. Mirsaeidi, D. M. Said, M. W. Mustafa *et al*., "A protection strategy for micro-grids based on positive-sequence component," *IET Renewable Power Generation*, vol. 9, no. 6, pp. 600-609, Mar. 2015.

[28] A. P. Apostolov, D. Tholomier, and S. H. Richards, "Superimposed components based sub-cycle protection of transmission lines," in *Proceedings of IEEE PES Power System Conference and Exposition*, New York, USA, Oct. 2004, pp. 592-597.

[29] G. Benmouyal and J. Roberts, "Superimposed quantities: their true nature and application in relays," in *Proceedings of the 26th Annual Western Protection Relay Conference*, Spokane, USA, Oct. 1999, pp. 1-18.

[30] E. Sedoyeka, Z. Hunaiti, M. A. Nabhan *et al*., "WiMAX mesh networks for underserved areas," in *Proceedings of International Conference on Computer System Applications*, Doha, Qatar, Mar. 2008, pp. 1070-1075.

[31] T. S. Basso and R. DeBlasio, "IEEE 1547 series of standards: interconnection issues," *IEEE Transactions on Power Electronics*, vol. 19, no. 5, pp. 1159-1162, Sept. 2004.

[32] K. Sarwagya, S. De, and P. K. Nayak, "High-impedance fault detection in electrical power distribution systems using moving sum approach," *IET Science Measurement and Technology*, vol. 12, no. 1, pp. 1-8, Aug. 2017.

[33] A. Ghaderi, H. A. Mohammadpour, H. L. Ginn *et al*., "High-impedance fault detection in the distribution network using the time-frequency-based algorithm," *IEEE Transactions on Power Delivery*, vol. 30, no. 3, pp. 1260-1268. Jun. 2015.

Bhatraj Anudeep received the B.Tech. degree in electrical engineering from Arjun College of Technology and Sciences, Hyderabad, India, in 2012, the M.Tech. degree in power system engineering from the T. R. R. College of Engineering and Technology, Hyderabad, India, in 2014, and is currently pursuing the Ph.D. degree at Indian Institute of Technology (Indian School of Mines) Dhanbad, Dhanbad, India. His research interests include electric power distribution system protection, control, and monitoring.

Paresh Kumar Nayak received the Ph.D. degree in electrical engineering from Indian Institute of Technology Kharagpur, Kharagpur, India, in 2014. He is currently an Assistant Professor at the Department of Electrical Engineering, Indian Institute of Technology (Indian School of Mines) Dhanbad, Dhanbad, India. His research interests include power system relaying, control, and protection of smart distribution systems.